

# Pattern stability in reaction–diffusion systems depends on path entropy\*

Eric R. Heller<sup>1,2,†</sup> and David T. Limmer<sup>1,2,3,‡</sup>

<sup>1</sup>*Department of Chemistry, University of California, Berkeley, 94720 Berkeley, USA*

<sup>2</sup>*Chemical Sciences and Materials Sciences Divisions,  
Lawrence Berkeley National Laboratory, Berkeley, CA, USA*

<sup>3</sup>*Kavli Energy NanoSciences Institute, Berkeley, CA, USA*

(Dated: March 13, 2026)

Reaction–diffusion systems driven far from thermodynamic equilibrium through the injection of energy can support multiple distinct spatial patterns that persist as long-lived dynamical phases. The stability of these metastable phases is not determined by thermodynamics, but by the transition paths connecting them. At finite particle numbers, intrinsic stochasticity induces rare transitions between competing patterns, rendering continuum mean-field descriptions insufficient, while exact stochastic simulations become computationally prohibitive in spatially extended systems. Here, we develop a nonequilibrium instanton framework that enables efficient computation of transition rates between metastable patterns from a single optimal transition path and its fluctuations. Using this theoretical framework, we show that an effective entropy in path space can qualitatively alter stability at finite particle numbers by increasing the exit rates of metastable patterns. By studying models of varying complexity, this work establishes path entropy as a key organizing principle for nonequilibrium pattern formation.

In equilibrium, the stability of a phase is determined by its free energy, which reflects a delicate balance between energetic and entropic contributions. Accordingly, the accurate prediction of equilibrium phase diagrams requires consideration of both quantities, as they jointly determine the complex structures that emerge [1, 2]. Nonequilibrium steady states can exhibit similarly intricate behavior [3–5]. Reaction–diffusion systems, for instance, sustain a wide variety of dynamic patterns whose organization can be tuned through external control parameters [6, 7]. Away from equilibrium, however, stability is no longer characterized by a static thermodynamic potential such as the free energy, but instead by dynamical properties like the lifetime of a metastable state [8–10]. The rates of transitions between metastable states depend sensitively on the ensemble of pathways connecting them, including both their likelihoods and their multiplicities. Using recently developed computational approaches based on nonequilibrium instanton theory [11–17], we demonstrate how the entropy in path space, the diversity of transition pathways, can shape the phase behavior of reaction–diffusion systems.

Reaction–diffusion models are used across the physical and biological sciences because they capture a minimal but universal structure of local transformation and spatial transport. Most commonly, these models are formulated using deterministic partial differential equations [18]. Within this framework, phase behavior and pattern formation, including Turing instabilities, propagating fronts, and domain formation, are studied through linear stability analysis of homogeneous steady states, with broad applications in biological and nonequilibrium

pattern formation [6, 7, 19–21]. While such descriptions capture typical spatiotemporal dynamics, they neglect the intrinsic stochasticity arising from the discrete and probabilistic nature of reactivity, which can qualitatively alter phase stability, particularly through rare, noise-induced transitions between metastable states [22–27]. Exact stochastic descriptions based on the reaction–diffusion master equation account for these effects, but their study is typically confined to numerical simulations that remain computationally prohibitive for spatially extended systems [28–31]. As a consequence, little is generally understood concerning the role of noise in shaping the phase diagrams of spatially extended nonequilibrium reaction–diffusion systems.

In order to bridge the gap between continuum mean-field descriptions and exact stochastic simulations, it is natural to focus on the rare transitions that control phase stability in noisy reaction–diffusion systems. In the weak-noise limit, these transitions are dominated by the optimal transition path or *instanton*, allowing transition rates to be computed from a single trajectory. Instanton approaches therefore provide an efficient route to determining the stability of dynamical phases in nonequilibrium reaction–diffusion systems and can be used to predict phase stability by comparing instanton actions for forward and backward transitions between metastable states. Actions play a role analogous to energy barriers in equilibrium systems, but unlike equilibrium barriers, the actions for forward and backward transitions are not related by detailed balance [16, 32]. However, just as equilibrium phase stability depends not only on energy but also on entropy, the action alone does not fully determine nonequilibrium stability at finite noise. As illustrated schematically in Fig. 1, path entropy can be essential for predicting accurate nonequilibrium phase diagrams. By accounting for Gaussian fluctuations around the optimal path, we are able to incorporate the local entropy in path

\* Supplemental material available

† [hellere@berkeley.edu](mailto:hellere@berkeley.edu)

‡ [dlimmer@berkeley.edu](mailto:dlimmer@berkeley.edu)

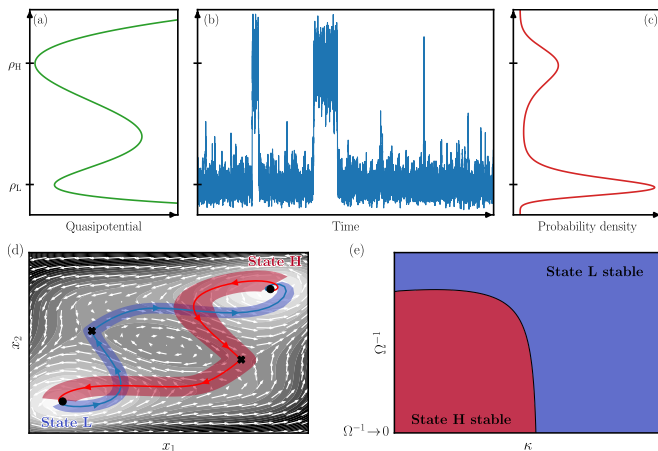


FIG. 1. Overview of how transition path entropy can alter stability of metastable states in nonequilibrium systems. (a) Effective-action or quasipotential landscape along a one-dimensional order parameter, indicating that the high-density state ( $\rho_H$ ) is favored in the absence of noise,  $\Omega \rightarrow \infty$ . (b) A representative stochastic trajectory and (c) the corresponding steady-state probability density show that, at sufficiently strong noise, the low-concentration state ( $\rho_L$ ) is more stable due to entropic enhancement of the  $\rho_H \rightarrow \rho_L$  transition. (d) Two-dimensional representation of the system in concentration space, showing an underlying double-well potential (color map) together with a nonconservative force field (stream plot). The forward (blue) and backward (red) optimal transition paths differ because detailed balance is broken. Broader fluctuations (transparent tubes) around the backward path indicate a larger statistical weight in path space, favoring it entropically at finite noise. (e) Schematic nonequilibrium phase diagram as a function of a system parameter  $\kappa$  and the noise strength  $\Omega^{-1}$ . In the zero-noise limit ( $\Omega^{-1} \rightarrow 0$ ), stability follows from the action, whereas at finite noise, path entropy can qualitatively alter stability and eliminate the phase transition altogether.

space into pattern stability.

We first outline the instanton-based approach used to analyze rare transitions in nonequilibrium reaction–diffusion systems. We then apply this framework to two representative models, a spatial Schlögl model [33] and an experimentally inspired competing enzyme network [34], to demonstrate how path entropy influences phase stability. Finally, we compare the path-based insights obtained for both systems to identify generic and system-specific features for system-size-dependent and particle-number-dependent stabilization of dynamic nonequilibrium phases.

## INSTANTONIC RATES OF REACTION–DIFFUSION SYSTEMS

We study reaction–diffusion systems in the limit where their dynamics are described by a chemical Langevin equation [35, 36]. Such a formulation assumes that the discrete Poissonian jump processes accompanying indi-

vidual reactive events are well approximated by a Gaussian stochastic process in continuous state space. The chemical Langevin equation is valid when copy numbers  $n^{(s)}$  of reactive molecular species  $s$  within some correlation volume  $\xi^d$  in  $d$  dimensions are large but finite, and when many reactions occur over a characteristic correlation time  $\tau$ . The resultant equation of motion for a multi-component density field is

$$\dot{\rho}(\mathbf{x}, t) = \mathbf{F}[\rho(\mathbf{x}, t)] + D\nabla^2\rho(\mathbf{x}, t) + \Omega^{-1/2}\mathbf{\Lambda}[\rho(\mathbf{x}, t)]\eta(\mathbf{x}, t), \quad (1)$$

where  $\rho(\mathbf{x}, t)$  denotes the vector of continuous concentrations for each species  $\rho^{(s)} = n^{(s)}/\Omega\xi^d$  in physical space  $\mathbf{x}$ , and  $\eta$  is a vector of independent Gaussian white noises, one for each reaction noise channel  $r$ , with zero mean and correlations  $\langle \eta_r(\mathbf{x}, t)\eta_{r'}(\mathbf{x}', t') \rangle = \delta_{rr'}\delta(\mathbf{x}-\mathbf{x}')\delta(t-t')$ . The diffusion is conservative and ideal with diffusion constant  $D$ . The deterministic drift  $\mathbf{F}$  and noise matrix  $\mathbf{\Lambda}$  encode the effects of reactions and a measure of their fluctuations. The scale of the noise depends on the characteristic particle number  $\Omega$  within a correlation volume  $\xi^d$ , and we consider a limit where particle number fluctuations due to reactions are the dominant source of noise, so we neglect noise from diffusion. In the  $\Omega \rightarrow \infty$  limit, the dynamics reduce to deterministic mass-action kinetics, whereas at finite noise, qualitatively different behavior can emerge, including rare transitions between metastable states.

In order to characterize rare transitions between metastable states, we employ nonequilibrium instanton theory, which provides an asymptotic expression for transition rates in the weak-noise regime. Instanton theory identifies the optimal transition path between metastable states that minimizes the action

$$S[\rho(\mathbf{x}, t)] = \frac{1}{2} \int d\mathbf{x} \int dt [\dot{\rho} - \mathbf{v}(\rho)]^T \chi^{-1}(\rho) [\dot{\rho} - \mathbf{v}(\rho)], \quad (2)$$

with  $\mathbf{v}[\rho(\mathbf{x}, t)] = \mathbf{F}[\rho(\mathbf{x}, t)] + D\nabla^2\rho(\mathbf{x}, t)$  and  $\chi[\rho(\mathbf{x}, t)] = \mathbf{\Lambda}[\rho(\mathbf{x}, t)]\mathbf{\Lambda}^T[\rho(\mathbf{x}, t)]$ . The resulting rate constant takes the asymptotic form

$$k = A \ell^f \Omega^{f/2} e^{-\Omega S[\bar{\rho}]}, \quad \left. \frac{\delta S}{\delta \rho} \right|_{\rho=\bar{\rho}} = 0, \quad (3)$$

where the action  $S[\bar{\rho}]$  governs the exponential scaling of the rate and generalizes the notion of a barrier height in equilibrium systems. The prefactor  $A$  captures fluctuations around the optimal path. Since the transition paths may involve the formation of interfaces with translational symmetry, we separately account for the effect of  $f$  translational Goldstone modes with  $\ell$  the linear system size in each spatial direction and  $\ell^f$  as the measure of the associated symmetry manifold, area for  $f=2$ , length for  $f=1$ , or dimensionless for  $f=0$ . This expression for the rate, its implication for stability in reaction–diffusion systems, and its efficient numerical evaluation, represent the major contributions of this work.

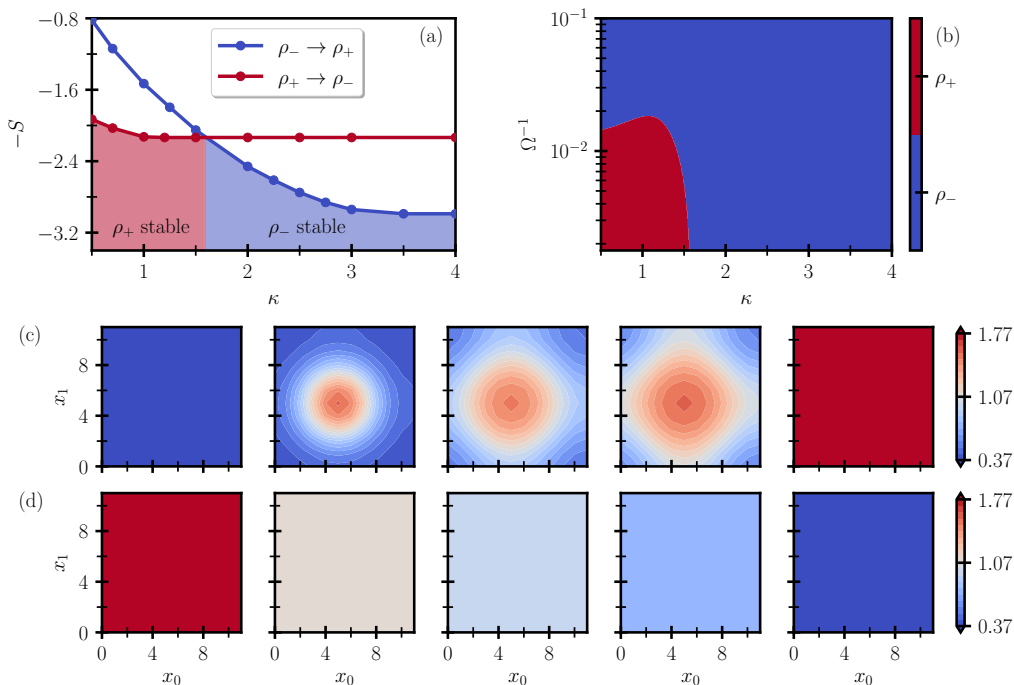


FIG. 2. (a) Instanton actions for the forward (blue) and backward (red) transitions between the high- and low-concentration states of the  $2d$  Schlögl model defined in the text. (b) Stability diagram, indicating the more stable phase as a function of  $\kappa = D\tau/\xi^2$  and  $\Omega$  based on the NEQI rate constants for the forward and backward transitions. Snapshots along the instantons of the forward (c) and backward (d) transitions at  $\kappa = 1.5$  with the color map indicating molecule concentration, where  $\rho_-\xi^2 \approx 0.37$  and  $\rho_+\xi^2 \approx 1.77$ . The coordinates  $x_0$  and  $x_1$  span the two-dimensional domain in units of  $\xi$ .

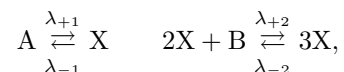
Generically, the steady-state distribution of a nonequilibrium system is a complex function of its dynamical variables. However, when the dynamics exhibit long-lived metastable states, the behavior can be described by coarse-grained transition rates between those states. The rates we quantify between metastable phases of reaction–diffusion systems in Eq. 3 are precisely those that enter such a description. In this limit, the population of any metastable state is inversely proportional to the net rate at which it is exited. By deducing a physically transparent form for these exit rates, we therefore obtain a means of understanding stability in nonequilibrium systems. Most previous applications inferred stability from differences in the instanton action, corresponding to the exponential scaling limit [16]. For example, large instanton actions yield small exit rates and therefore more stable phases. Here, we extend this description by explicitly evaluating the fluctuation prefactor. This prefactor encodes an effective entropy in path space that can compete with the action at finite noise, as illustrated schematically in Fig. 1. Higher path entropy, generated either through large fluctuations around the optimal path or through a larger number of Goldstone modes, leads to larger exit rates and less stable phases.

In the following sections, we apply this framework to a spatial Schlögl model and to a competing enzyme network, demonstrating how path entropy qualitatively modifies phase stability in driven reaction–diffusion sys-

tems. Both systems are considered in two dimensions in the main text, and additional simulations in one and zero dimensions are shown in the SI. To numerically evaluate the transition rates from the chemical Langevin description, we discretize space and time and employ our recent nonequilibrium instanton (NEQI) framework [11]. Space is divided into  $L$  voxels of length  $\xi$ , each containing a network of local chemical reactions, while adjacent compartments are coupled by diffusive particle hops with dimensionless microscopic rate  $\kappa = D\tau/\xi^2$ . Details of the implementation are presented in the SI. Throughout, we compare our NEQI results with simulations of the full stochastic dynamics governed by a reaction–diffusion master equation, as shown in the SI, which describes the evolution of discrete particle numbers for each species through Poissonian reaction and diffusion events and can be simulated using kinetic Monte Carlo. Unless stated otherwise, we work in unit systems where  $\xi = \tau = 1$ .

## SPATIALLY EXTENDED SCHLÖGL MODEL

We first apply our approach to a spatially extended version of the classical Schlögl model [33],



where the concentrations of species A and B are held fixed by chemostats, and only a single density associated with species X evolves in time. For suitable reaction parameters, the deterministic drift of the corresponding chemical Langevin equation,  $F(\rho) = \lambda_{+1} + \lambda_{+2}\rho^2 - \lambda_{-2}\rho^3 - \lambda_{-1}\rho$ , exhibits bistability between a low-concentration state  $\rho_-$  and a high-concentration state  $\rho_+$ . Although the local drift can be written as the gradient of a double-well potential, the state-dependent noise violates the fluctuation-dissipation relation, and detailed balance is broken. As a consequence, the Schlögl model is one of the simplest nonequilibrium chemical systems that exhibits bistability, making it a foundational model for understanding pattern formation.

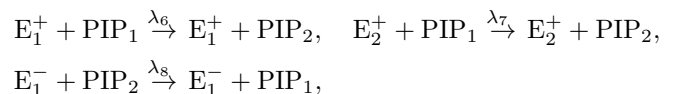
The instanton actions for the forward and backward transitions between the two metastable states are shown in Fig. 2(a) as a function of the microscopic diffusion constant. For small  $D$ , or  $\kappa$ , the high-concentration state is favored, whereas at large  $D$  the low-concentration state becomes more stable, with a crossover near  $\kappa = D\tau/\xi^2 \approx 1.6$ . This diffusion-constant-dependent crossover in stability is consistent with previous results for one-dimensional Schlögl models [16, 32]. In the strong-diffusion limit, the actions plateau as the system behaves effectively as a single homogeneous compartment, whereas at  $D = 0$  each point in space evolves independently. At intermediate values of  $D$ , however, the forward and backward transitions proceed via qualitatively different mechanisms. As shown in Fig. 2(c-d), the forward transition from  $\rho_-$  to  $\rho_+$  nucleates a localized critical droplet, leading to a translational degeneracy of the instanton in two dimensions and two corresponding Goldstone modes,  $f = 2$ . In contrast, the backward transition at the same  $D$  follows a spatially homogeneous mechanism,  $f = 0$ , and favors interface formation only at much slower diffusion. These disparate mechanisms reflect the breaking of detailed balance and imply markedly different fluctuations around their optimal paths.

Including the fluctuation prefactor allows us to compute absolute transition rates and construct the stability diagram shown in Fig. 2(b) as a function of  $D$  and the noise strength  $\Omega^{-1}$ . While the instanton action alone predicts a diffusion-dependent stability crossover, the inclusion of path entropy qualitatively modifies this picture. Below a characteristic particle number,  $\Omega \lesssim 90$ , the low-concentration state remains stable for all  $D$ , and the predicted crossover disappears. The disappearance of the action-based crossover at finite noise illustrates that stability in nonequilibrium reaction-diffusion systems cannot be inferred from the exponential action alone. Fluctuation effects in path space can offset substantial differences in action, leading to qualitatively different nonequilibrium phase diagrams. Note that the single-path approximation for the prefactor breaks down in a narrow regime in  $D$  where competing mechanisms become comparable. To alleviate this, we interpolate smoothly between the logarithmic rate constants obtained on either side of this regime (see SI). While the chemical Langevin

equation does not in general reproduce the Poissonian tails that can govern rare events in reaction-diffusion systems [37, 38], we find that for the Schlögl model, our results agree quantitatively with direct simulations of a corresponding reaction-diffusion master equation (SI).

## COMPETING ENZYME NETWORK

Building on the insights from the Schlögl model, we next consider a more realistic nonequilibrium reaction-diffusion system inspired by the competitive kinase-phosphatase network studied experimentally in Ref. [34]. In this system, the interconversion of the membrane lipids phosphatidylinositol-4-phosphate (PIP<sub>1</sub>) and phosphatidylinositol-4,5-phosphate (PIP<sub>2</sub>) is catalyzed by membrane-bound kinase and phosphatase enzymes. Kinetic measurements identified the relevant species as the phosphatase in solution ( $E_0^-$ ) and singly bound to PIP<sub>1</sub> ( $E_1^-$ ), as well as the kinase in solution ( $E_0^+$ ) and singly and doubly bound to PIP<sub>2</sub> ( $E_1^+$ ,  $E_2^+$ ) [34]. Under ATP consumption, the kinase (phosphatase) catalyzes phosphorylation (dephosphorylation) according to



coupled to membrane binding and unbinding reactions, as illustrated in Fig. 3. For a fixed total lipid density, this system contains four relevant concentration fields, associated with the enzymes  $E_1^+$ ,  $E_2^+$  and  $E_1^-$ , and the imbalance of PIP<sub>2</sub> over PIP<sub>1</sub>.

For a given set of rates and lipid density motivated by experimental observations, detailed in the Materials and Methods section, this reaction network supports two metastable states dominated by either PIP<sub>1</sub> or PIP<sub>2</sub>, consistent with observations showing macroscopic bistability in Ref. [34]. In contrast to the Schlögl model, bistability here emerges from feedback between multiple interacting species. High concentrations of PIP<sub>1</sub> or PIP<sub>2</sub> are directly coupled to increased populations of membrane-bound enzymes that catalyze the production of the respective lipid, reinforcing the dominant state. The en-

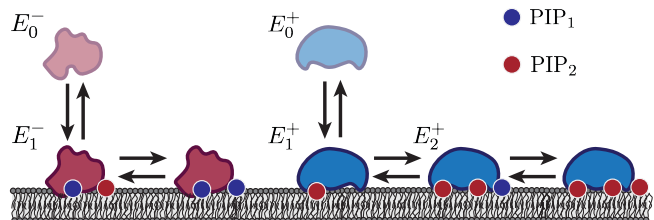


FIG. 3. Schematic representation of the competing enzyme model studied in this work. Lipid membrane containing PIP<sub>1</sub> and PIP<sub>2</sub> in contact with kinase and phosphatase enzymes in solution that can bind and catalyze lipid interconversion under ATP consumption.

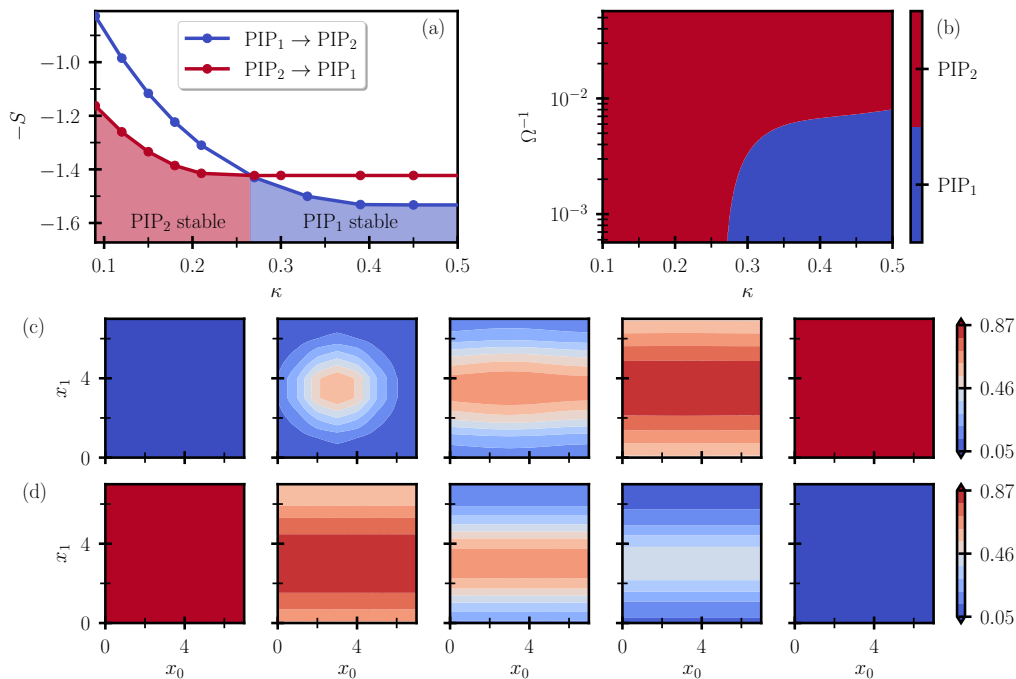


FIG. 4. (a) Instanton actions for the forward (blue) and backward (red) transitions between the uniform PIP<sub>1</sub>- and PIP<sub>2</sub>-dominated states of the 2D competitive enzyme model defined in the text. (b) Stability diagram, indicating the more stable phase as a function of  $\kappa = D\tau/\xi^2$  and  $\Omega$  based on the NEQI rate constants for the forward and backward transitions. Snapshots along the instantons of the forward (c) and backward (d) transitions at  $\kappa = 0.15$  with the color map indicating the PIP<sub>2</sub> concentration, where the PIP<sub>1</sub>- and PIP<sub>2</sub>-dominated states exhibit a PIP<sub>2</sub> concentration of  $\rho^{\text{PIP}_2}\xi^2 \approx 0.05$  and  $\rho^{\text{PIP}_2}\xi^2 \approx 0.87$ . The coordinates  $x_0$  and  $x_1$  span the two-dimensional domain in units of  $\xi$ .

zyme system contains only first- and second-order reactions, leading to a drift in the reaction–diffusion equations that is at most quadratic in the species concentrations. The bistability therefore does not arise from a double-well structure obtained by integrating the drift, as in the Schlögl model, but from genuinely nonequilibrium feedback between different chemical species encoded in a strongly nonconservative drift. The enzyme system is thus far from equilibrium both because it violates the fluctuation–dissipation relation and because its deterministic drift cannot be derived from a potential.

The phase stability in the spatially extended enzyme system in the limit of zero noise can be understood by optimizing instantons for the forward PIP<sub>1</sub>  $\rightarrow$  PIP<sub>2</sub> and backward PIP<sub>2</sub>  $\rightarrow$  PIP<sub>1</sub> transitions as a function of  $D$ . The resulting actions are shown in Fig. 4(a). As in the Schlögl model, the exponential scaling predicts a diffusion-dependent crossover of the more stable state. In the strong-diffusion limit, both actions plateau and PIP<sub>1</sub> is favored, whereas at small  $D$  the stronger diffusion dependence of the forward transition leads to an inversion of stability.

The corresponding instantons shown in Fig. 4(c–d) reveal that, in addition to uniform and droplet-forming paths, mechanisms with one-dimensional stripe-like interfaces appear due to finite system size, similar to mechanisms observed in driven nucleation problems [39].

These distinct pathways are associated with markedly different fluctuation structures in path space, which are reflected in the stability diagram in Fig. 4(b). As in the Schlögl model, the crossover predicted from the action alone is recovered in the  $\Omega \rightarrow \infty$  limit. At finite particle numbers, however, fluctuation effects qualitatively modify the phase diagram. For  $\Omega \lesssim 100$ , the PIP<sub>2</sub>-dominated state becomes entropically favored over a broad range of diffusion constants.

As shown in Fig. SI.9 of the SI, the NEQI+chemical Langevin approach captures the trends seen in a corresponding master equation study, but differs by an approximately  $\Omega$ -independent, system-size-dependent multiplicative factor, slightly overstabilizing the PIP<sub>1</sub>-dominated state. This deviation reflects a limitation of the Langevin approximation when certain species occur at low copy numbers, where the discrete Poissonian statistics of the reaction and diffusion processes matter. Because the error is systematic and relatively small compared to the exponential action differences, the NEQI results still provide a reliable estimate of the phase stability. Indeed, as the Langevin approximation slightly underestimates the stability of the PIP<sub>2</sub> state relative to master equation dynamics, the true entropy-driven stabilization is expected to be even stronger. The phase diagram in Fig. 4(b) should therefore be interpreted as a lower bound on fluctuation-induced stabilization of the

PIP<sub>2</sub> state.

## ROLE OF PATH ENTROPY IN STABILITY

The Schlögl model [Fig. 2(b)] and the enzyme model [Fig. 4(b)] yield qualitatively similar stability diagrams, despite their very different reaction networks. In both cases, the exponential-scaling limit  $\Omega \rightarrow \infty$  predicts a diffusion-dependent crossover of the most stable state. Identifying the PIP<sub>2</sub>-dominated state as the high-concentration (and therefore high-noise) state for our parameters, we observe that in both systems the high-noise state is favored at slow diffusion, whereas the low-noise state dominates in the homogeneous limit. The origin of this diffusion-dependent bistability lies in the interplay between deterministic drift and state-dependent noise. For the parameters considered, the drift alone favors the high-density state. At small  $D$ , the relevant saddle configuration is a small bubble of the high-density phase embedded in a low-density background. Such a localized nucleus can form and grow more easily than the reverse process, which would require the creation of an extended low-density region within a high-density background. Consequently, the high-density state becomes more stable as  $D$  decreases. In the homogeneous  $D \rightarrow \infty$  limit, however, spatial structure is suppressed. As shown for the Schlögl model in Fig. SI.1 of the SI, the larger state-dependent noise amplitude modifies the effective quasipotential and overcompensates the drift advantage, stabilizing the low-density state overall. The diffusion-dependent crossover therefore reflects a shift between a bubble-nucleation regime dominated by the drift and a homogeneous limit dominated by the state-dependent noise.

Finite particle numbers modify this action-based picture of stability. In the limit of two metastable states, stability is controlled by rate ratios, not by action differences alone. It is therefore natural to define an effective nonequilibrium stability difference  $\Delta\Phi(\Omega) = -\Omega^{-1} \ln k_{\text{fw}}/k_{\text{bw}}$  in terms of the forward and backward rate constants  $k_{\text{fw}}$  and  $k_{\text{bw}}$ . Using our form of the rate [Eq. (3)], this yields

$$\Delta\Phi(\Omega) = S_{\text{fw}} - S_{\text{bw}} - \Omega^{-1} \left[ \frac{1}{2}(f_{\text{fw}} - f_{\text{bw}}) \ln \Omega + \ln \left( \frac{A_{\text{fw}} \ell_{\text{fw}}^{f_{\text{fw}}}}{A_{\text{bw}} \ell_{\text{bw}}^{f_{\text{bw}}}} \right) \right], \quad (4)$$

which makes explicit that the instanton action  $S$  competes with entropic contributions from the prefactor. The prefactor is decomposed into contributions from translational symmetry modes and the fluctuation spectrum of all the remaining modes. The diffusion-dependent crossover predicted from  $S$  alone therefore becomes visible only once  $\Omega$  is sufficiently large that action differences dominate over potentially large prefactor ratios. At smaller  $\Omega$ , entropic advantages in path space can over-

whelm the action difference and eliminate the crossover altogether.

The two models differ in which basin is entropically favored because the difference in path entropy between forward and backward transitions is dominated by different factors. In the enzyme system, the PIP<sub>1</sub>  $\rightarrow$  PIP<sub>2</sub> transition strongly favors interface formation and exhibits soft interfacial modes that enhance the prefactor, entropically stabilizing the high-noise PIP<sub>2</sub> state. In the Schlögl model, by contrast, the low- and high-density basins differ more strongly in their intrinsic noise amplitudes. The larger effective noise in the high-density state softens fluctuations along the optimal paths in a way that entropically favors the high-to-low transition, thus entropically stabilizing the low-density state.

Overall, the comparison highlights a general principle for driven reaction–diffusion systems. Diffusion controls stability through the spatial geometry of the optimal bottleneck, bubble nucleation versus homogenized rearrangement, while finite particle numbers introduce path entropy as an additional stabilizing mechanism that depends on interfacial degeneracies, soft fluctuation modes, and state-dependent noise along the transition. Which effect dominates is system- and parameter-dependent and cannot be inferred reliably from the action or from geometry arguments alone. Quantitative predictions therefore require rate theories like NEQI to treat both the optimal paths and their fluctuations on equal footing.

## CONCLUDING REMARKS

In summary, we have shown that phase stability in driven reaction–diffusion systems is governed not only by the optimal transition pathways between metastable states but also by the fluctuations around them. Diffusivity and system size control whether rare transitions are dominated by bubble nucleation or homogeneous rearrangements. In both the Schlögl and enzyme models, the diffusion-dependent crossover in the most stable phase predicted from the instanton action alone emerges only in the weak-noise limit. At finite particle numbers, entropic contributions associated with interfacial degeneracies and state-dependent noise can suppress or reverse this crossover. These results highlight path entropy as a central organizing principle for nonequilibrium phase stability. We suspect these effects are relevant for a broad range of systems in chemistry, molecular biology, and ecology where small spatial scales result in finite population sizes [40–43].

## MATERIALS AND METHODS

In order to study the chemical Langevin equation [Eq. (1)] numerically, we explicitly partition space into  $L$  correlation volumes of size  $\xi^d$ . Within voxel  $l$ , the concentration of species  $s$  is  $\rho_l^{(s)} = n_l^{(s)}/\Omega\xi^d$ , where  $n_l^{(s)}$  de-

notes the corresponding particle number. The chemical Langevin equation then reads

$$\begin{aligned} \dot{\rho}_l^{(s)} = & \sum_{r=1}^R w_r^{(l)}(\rho) \nu_r^{(l,s)} + \sum_{m \in nn(l)} \kappa^{(s)}(\rho_m^{(s)} - \rho_l^{(s)}) \\ & + \Omega^{-1/2} \sum_{r=1}^R \sqrt{w_r^{(l)}(\rho)} \nu_r^{(l,s)} \eta_r^{(l)}(t), \end{aligned} \quad (5)$$

where  $\rho$  collects concentrations in all voxels and species,  $w_r^{(l)}$  are reaction propensities, and  $\nu_r^{(l,s)}$  are stoichiometric changes of species  $s$  in voxel  $l$  under reaction  $r$ . For elementary reactions, propensities follow mass-action kinetics and are given by products of reactant concentrations in voxel  $l$  multiplied by the corresponding rate constants  $\lambda_r$  [35]. Diffusion of species  $s$  occurs between neighboring voxels  $m \in nn(l)$  with microscopic diffusion constant  $\kappa^{(s)}$ . The Gaussian noise variables have zero mean and correlations  $\langle \eta_r^{(l)}(t) \eta_{r'}^{(l')}(t') \rangle = \xi^{-d} \delta_{rr'} \delta_{ll'} \delta(t-t')$ , where  $\xi^{-d} \delta_{ll'}$  represents the continuum noise correlation  $\delta(x-x')$  in Eq. (1) on a discrete voxel grid. The first two terms in Eq. (5) describe deterministic reaction and diffusion, while the final term represents multiplicative reaction noise obtained from approximating the reactive Poissonian jump processes of the reaction-diffusion master equation in the large- $\Omega$  limit. In the continuum notation of the main text, the deterministic drift and noise covariance in Eq. (5) recover  $v[\rho(x,t)] = F[\rho(x,t)] + D\nabla^2 \rho(x,t)$  and  $\chi[\rho(x,t)] = \mathbf{\Lambda}[\rho(x,t)] \mathbf{\Lambda}^T[\rho(x,t)]$ . In the SI, we detail the conditions under which the chemical Langevin equation provides an accurate approximation of the master equation for rare reactive events.

For numerical evaluation, the path action [Eq. (2)] is discretized into  $N$  segments with time step  $t_N = T/N$ ,

$$\begin{aligned} S_N(\rho) = & \frac{t_N}{2} \sum_{j=0}^{N-1} \xi^d \left[ \frac{\rho_{j+1} - \rho_j}{t_N} - v(\rho_j) \right]^T \\ & \times \chi^{-1}(\rho_j) \left[ \frac{\rho_{j+1} - \rho_j}{t_N} - v(\rho_j) \right], \end{aligned} \quad (6)$$

where,  $\rho$  contains all system copies or *beads*,  $\rho_j$ , along the path with endpoints fixed at the reactant fixed point and the unstable saddle separating the metastable states. Each bead configuration is a vector containing the density in every correlation volume. The quadratic form in Eq. (6) therefore corresponds to evaluating the spatial integral in Eq. (2) as a discrete sum. The instanton is obtained by minimizing this action with respect to the intermediate bead configurations  $\rho_1, \dots, \rho_{N-1}$  using Newton-Raphson-type optimizers [11, 44, 45]. The results must be converged with respect to  $T$  and  $N$ , which can be sped up by allowing variable time steps [11] or transforming to a path-length coordinate [13].

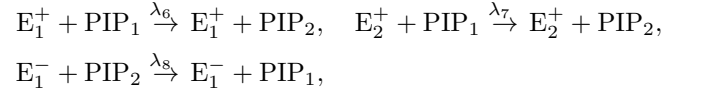
From the instanton, the rate constant is evaluated as

[11]

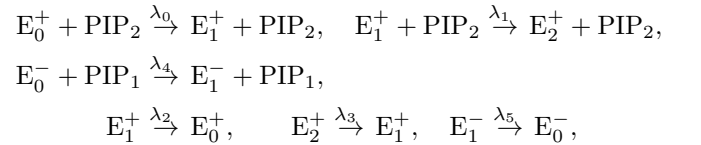
$$k \sim \frac{\zeta}{2\pi t_N} \sqrt{\frac{B_t \xi^{2d}}{t_N p_f^2 \Sigma}} e^{-\Omega S_N}, \quad (7)$$

where  $\Sigma = \det'[t_N \nabla_N^2 S_N / \xi^d] \prod_{j=1}^N \det[\chi(\rho_j)]$  encodes fluctuations around the optimal path,  $\nabla_N = (\partial/\partial \rho_1, \dots, \partial/\partial \rho_N)$  represents the gradient with respect to bead coordinates,  $\nabla_N^2 S_N$  is the Hessian of the discretized action, and the prime indicates omission of zero eigenvalues from temporal and spatial symmetries as well as the projected reaction coordinate. The magnitude of the endpoint momentum is denoted by  $p_f$ , and the Jacobians  $B_t$  and  $\zeta$  arise from integration over zero modes and are detailed in the SI. The instanton results were converged by systematically increasing the number of beads  $N$  until doubling  $N$  changed the action by less than 1% and the prefactor by less than 20%, requiring between 2000 and 12000 beads depending on system parameters. Convergence with respect to the total propagation time  $T$  was verified by repeating the calculations at increasing  $T$  and by confirming a numerically vanishing eigenvalue associated with time-translation symmetry.

The two-dimensional Schlögl model is defined on a  $12 \times 12$  grid with periodic boundary conditions and reaction rates  $\lambda_{+1}\tau = 0.73$ ,  $\lambda_{+2}\tau = 3.7$ ,  $\lambda_{-1}\tau = 3.2$ ,  $\lambda_{-2}\tau = 1.2$ . In addition to catalytic lipid interconversion reactions



the enzyme model includes membrane binding and unbinding reactions



as well as weak non-specific binding reactions introduced to ensure ergodicity



Throughout, we choose the following rates for the first-order reactions  $\lambda_0\tau = 1$ ,  $\lambda_2\tau = 4$ ,  $\lambda_3\tau = 0.1$ ,  $\lambda_4\tau = 0.05$ ,  $\lambda_5\tau = 0.2$ ,  $\lambda_9 = 0.1\lambda_0$ ,  $\lambda_{10} = 0.1\lambda_4$ , and the second-order reactions  $\lambda_1\tau = 0.1635$ ,  $\lambda_6\tau = 0.556$ ,  $\lambda_7 = \lambda_8 = 4\lambda_6$ , where the enzyme concentrations in solution ( $E_0^+$ ,  $E_0^-$ ) are absorbed into pseudo-first-order rate constants. The total lipid number is conserved, and the total lipid density is fixed at  $\rho_{\text{tot}}\xi^2 = 1$ .

In the  $L$ -voxel enzyme model, conservation of the total lipid density implies that the noise matrix  $\chi(\rho)$  is singular, since fluctuations in  $\text{PIP}_1$  and  $\text{PIP}_2$  are linearly dependent. To evaluate  $\chi^{-1}$  in the action, we introduce a small regularization parameter  $\epsilon$  that lifts

the null mode associated with lipid conservation and leads to  $\epsilon$ -independent results for small but finite values. The details of the regularization procedure are provided in the SI.

**Acknowledgments:** ERH is grateful for financial support from the Swiss National Science Foundation

through Grant 214242. DTL was supported by the Condensed Phase and Interfacial Molecular Science Program (CPIMS) of the U.S. Department of Energy under contract no. DEAC02-05CH11231. This research used the Lawrence Livermore computational cluster resource provided by the IT Division at Lawrence Berkeley National Laboratory under the same contract.

- 
- [1] D. Chandler, *Introduction to Modern Statistical Mechanics* (Oxford University Press, New York, 1987).
- [2] P. M. Chaikin and T. C. Lubensky, *Principles of condensed matter physics* (Cambridge University Press, Cambridge, 1995).
- [3] D. T. Limmer, *Statistical mechanics and stochastic thermodynamics* (Oxford University Press, Oxford, 2024).
- [4] M. E. Cates and J. Tailleur, Motility-induced phase separation, *Annu. Rev. Condens. Ma. P.* **6**, 219 (2015).
- [5] T. Grafke, M. E. Cates, and E. Vanden-Eijnden, Spatiotemporal self-organization of fluctuating bacterial colonies, *Phys. Rev. Lett.* **119**, 188003 (2017).
- [6] A. M. Turing, The chemical basis of morphogenesis, *Philos. Trans. R. Soc. Lond. B. Biol. Sci.* **237**, 37 (1952).
- [7] M. C. Cross and P. C. Hohenberg, Pattern formation outside of equilibrium, *Rev. Mod. Phys.* **65**, 851 (1993).
- [8] M. I. Freidlin and A. D. Wentzell, *Random Perturbations Of Dynamical Systems*, 3rd ed. (Springer, Berlin Heidelberg, 2012).
- [9] L. Onsager and S. Machlup, Fluctuations and irreversible processes, *Phys. Rev.* **91**, 1505 (1953).
- [10] R. Graham, Statistical theory of instabilities in stationary nonequilibrium systems with applications to lasers and nonlinear optics, in *Springer Tracts in Modern Physics*, edited by G. Höhler (Springer, Berlin Heidelberg, 1973) pp. 1–97.
- [11] E. R. Heller and D. T. Limmer, Evaluation of transition rates from nonequilibrium instantons, *Phys. Rev. Res.* **6**, 043110 (2024).
- [12] E. Weinan, R. Weiqing, and E. Vanden-Eijnden, Minimum action method for the study of rare events, *Commun. Pure Appl. Math.* **57**, 637 (2004).
- [13] M. Heymann and E. Vanden-Eijnden, The geometric minimum action method: A least action principle on the space of curves, *Commun. Pure Appl. Math.* **61**, 1052 (2008).
- [14] T. Grafke, R. Grauer, and T. Schäfer, The instanton method and its numerical implementation in fluid mechanics, *J. Phys. A: Math. Theor.* **48**, 333001 (2015).
- [15] F. Bouchet and J. Reygner, Generalisation of the Eyring–Kramers transition rate formula to irreversible diffusion processes, *Ann. Henri Poincaré* **17**, 3499 (2016).
- [16] R. Zakine and E. Vanden-Eijnden, Minimum-action method for nonequilibrium phase transitions, *Phys. Rev. X* **13**, 041044 (2023).
- [17] J. Lehmann, P. Reimann, and P. Hänggi, Activated escape over oscillating barriers: The case of many dimensions, *Phys. Status Solidi B* **237**, 53 (2003).
- [18] J. Smoller, *Shock Waves and Reaction–Diffusion Equations*, 2nd ed., Grundlehren der mathematischen Wissenschaften, Vol. 258 (Springer-Verlag, New York, 1994).
- [19] S. Kondo and T. Miura, Reaction-diffusion model as a framework for understanding biological pattern formation, *Science* **329**, 1616 (2010).
- [20] A. L. Krause, E. A. Gaffney, P. K. Maini, and V. Klika, Modern perspectives on near-equilibrium analysis of turing systems, *Philos. Trans. Royal Soc. A* **379**, 10.1098/rsta.2020.0268 (2021).
- [21] Y. Karita, D. T. Limmer, and O. Hallatschek, Scale-dependent tipping points of bacterial colonization resistance, *Proc. Natl. Acad. Sci.* **119**, e2115496119 (2022).
- [22] D. A. McQuarrie, Stochastic approach to chemical kinetics, *J. Appl. Probab.* **4**, 413 (1967).
- [23] R. E. Lee DeVille, C. B. Muratov, and E. Vanden-Eijnden, Non-meanfield deterministic limits in chemical reaction kinetics, *J. Chem. Phys.* **124**, 10.1063/1.2217013 (2006).
- [24] T. Tian and K. Burrage, Stochastic models for regulatory networks of the genetic toggle switch, *Proc. Natl. Acad. Sci.* **103**, 8372 (2006).
- [25] G. Craciun, Y. Tang, and M. Feinberg, Understanding bistability in complex enzyme-driven reaction networks, *Proc. Natl. Acad. Sci.* **103**, 8697 (2006).
- [26] S. Smith and R. Grima, Spatial stochastic intracellular kinetics: A review of modelling approaches, *Bull. Math. Biol.* **81**, 2960 (2018).
- [27] A. A. Lee, W. Y. C. Huang, S. D. Hansen, N. H. Kim, S. Alvarez, and J. T. Groves, Stochasticity and positive feedback enable enzyme kinetics at the membrane to sense reaction size, *Proc. Natl. Acad. Sci.* **118**, 10.1073/pnas.2103626118 (2021).
- [28] D. T. Gillespie, A general method for numerically simulating the stochastic time evolution of coupled chemical reactions, *Journal of computational physics* **22**, 403 (1976).
- [29] D. T. Gillespie, Exact stochastic simulation of coupled chemical reactions, *The journal of physical chemistry* **81**, 2340 (1977).
- [30] D. T. Gillespie, Stochastic simulation of chemical kinetics, *Annu. Rev. Phys. Chem.* **58**, 35 (2007).
- [31] S. B. Nicholson and T. R. Gingrich, Quantifying rare events in stochastic reaction-diffusion dynamics using tensor networks, *Physical Review X* **13**, 041006 (2023).
- [32] S. Tănase-Nicola and D. K. Lubensky, Exchange of stability as a function of system size in a nonequilibrium system, *Phys. Rev. E* **86**, 040103 (2012).
- [33] C. Kim, A. Nonaka, J. B. Bell, A. L. Garcia, and A. Donev, Stochastic simulation of reaction-diffusion systems: A fluctuating-hydrodynamics approach, *J. Chem. Phys.* **146**, 124110 (2017).
- [34] S. D. Hansen, W. Y. C. Huang, Y. K. Lee, P. Bieling, S. M. Christensen, and J. T. Groves, Stochastic geometry sensing and polarization in a lipid kinase-phosphatase competitive reaction, *Proc. Natl. Acad. Sci.* **116**, 15013

- (2019).
- [35] D. T. Gillespie, The chemical langevin equation, *J. Chem. Phys.* **113**, 297 (2000).
- [36] N. G. V. Kampen, *Stochastic Processes in Physics and Chemistry*, 3rd ed. (North Holland, Amsterdam, 2007) p. 464.
- [37] M. Vellela and H. Qian, Stochastic dynamics and non-equilibrium thermodynamics of a bistable chemical system: the Schlögl model revisited, *J. R. Soc. Interface* **6**, 925 (2008).
- [38] J. Schüttler, R. L. Jack, and M. E. Cates, Effects of phase separation on extinction times in population models, *J. Stat. Mech.: Theory Exp.* **2024** (8), 083209.
- [39] M. Heymann and E. Vanden-Eijnden, Pathways of maximum likelihood for rare events in nonequilibrium systems: Application to nucleation in the presence of shear, *Phys. Rev. Lett.* **100**, 140601 (2008).
- [40] D. T. Limmer, A. W. Götz, T. H. Bertram, and G. M. Nathanson, Molecular insights into chemical reactions at aqueous aerosol interfaces, *Annu. Rev. Phys. Chem.* **75**, 111 (2024).
- [41] G. Birzu, O. Hallatschek, and K. S. Korolev, Fluctuations uncover a distinct class of traveling waves, *Proc. Natl. Acad. Sci.* **115**, E3645 (2018).
- [42] P. F. Hagolani, R. Zimm, M. Marin-Riera, and I. Salazar-Ciudad, Cell signaling stabilizes morphogenesis against noise, *Development* **146**, dev179309 (2019).
- [43] I. Hecht, D. A. Kessler, and H. Levine, Transient localized patterns in noise-driven reaction-diffusion systems, *Phys. Rev. Lett.* **104**, 158301 (2010).
- [44] J. O. Richardson, Ring-polymer instanton theory, *Int. Rev. Phys. Chem.* **37**, 171 (2018).
- [45] I. M. Ansari, E. R. Heller, G. Trenins, and J. O. Richardson, Instanton theory for Fermi's golden rule and beyond, *Phil. Trans. R. Soc. A* **380**, 20200378 (2022).